

LLaVA-RadZ: Can Multimodal Large Language Models Effectively Tackle Zero-shot Radiology Recognition?

Bangyan Li^{1*} Wenxuan Huang^{1*} Yunhang Shen² Yeqi Wang³
 Shaohui Lin^{1✉} Jingzhong Lin¹ Ling You¹ Yinqi Zhang¹
 Ke Li² Xing Sun² Yuling Sun^{1✉}
¹East China Normal University ²Tencent Youtu Lab. ³Northwest A&F University
 {libangyan2878, osilly0616, shaohuilin007, yulingsun.lv}@gmail.com

Abstract

Recently, multimodal large models (MLLMs) have demonstrated exceptional capabilities in visual understanding and reasoning across various vision-language tasks. However, MLLMs usually perform poorly in zero-shot medical disease recognition, as they do not fully exploit the captured features and available medical knowledge. To address this challenge, we propose **LLaVA-RadZ**, a simple yet effective framework for zero-shot medical disease recognition. Specifically, we design an end-to-end training strategy, termed **Decoding-Side Feature Alignment Training (DFAT)** to take advantage of the characteristics of the MLLM decoder architecture and incorporate modality-specific tokens tailored for different modalities, which effectively utilizes image and text representations and facilitates robust cross-modal alignment. Additionally, we introduce a **Domain Knowledge Anchoring Module (DKAM)** to exploit the intrinsic medical knowledge of large models, which mitigates the **category semantic gap** in image-text alignment. DKAM improves category-level alignment, allowing for accurate disease recognition. Extensive experiments on multiple benchmarks demonstrate that our LLaVA-RadZ significantly outperforms traditional MLLMs in zero-shot disease recognition and exhibits the state-of-the-art performance compared to the well-established and highly-optimized CLIP-based approaches.

1. Introduction

With the rapid advancement of deep learning technologies, an increasing number of studies have focused on their ap-

plications in medical disease diagnosis, yielding remarkable results [1–4]. However, these approaches typically rely on high-quality annotations provided by clinical experts. Unlike natural image datasets, annotating medical images is both costly and time-consuming. To address this challenge, recent research has explored methods based on paired medical images and textual reports, leveraging contrastive learning techniques. By minimizing the distance between paired samples while maximizing the distance between unpaired ones, these approaches enable zero-shot disease recognition, thereby reducing reliance on extensive medical data annotation to a certain extent.

In our in-depth investigation of advanced zero-shot disease recognition methods in the medical domain, we examined several representative models, including CARZero [5], MedKLIP [6], KAD [7], and MAVL [8]. While these methods have achieved significant performance improvements, they invariably incorporate external models or expert domain knowledge to some extent, rather than fully leveraging the models’ intrinsic understanding capabilities. Recently, multimodal large language models (MLLMs) [9–14] have demonstrated remarkable capabilities across various user-oriented vision-language tasks, such as image comprehension and reasoning, offering new possibilities for zero-shot disease recognition in medical applications. Among these, LLaVA-Med [15] has exhibited exceptional domain-specific medical knowledge in dialogue-based tasks, indicating that it possesses a certain degree of medical expertise. Therefore, building upon LLaVA-Med, we further explore its potential in zero-shot medical classification.

However, recent study [16] found that MLLMs (*i.e.*, LLaVA [11]) performed significantly worse than CLIP [17] on standard image classification tasks. To further validate this observation, we conducted zero-shot classification experiments using multiple MLLMs on five medical imaging datasets. The experimental results are consistent with previous findings, confirming that MLLMs exhibit sub-

*Equal contribution. Wenxuan Huang proposed the main idea and designed the experiments, contributing to the discussion of this paper. Bangyan Li refined and finalized the idea, implemented the code and experiments, and was responsible for writing the manuscript.

✉Corresponding author.

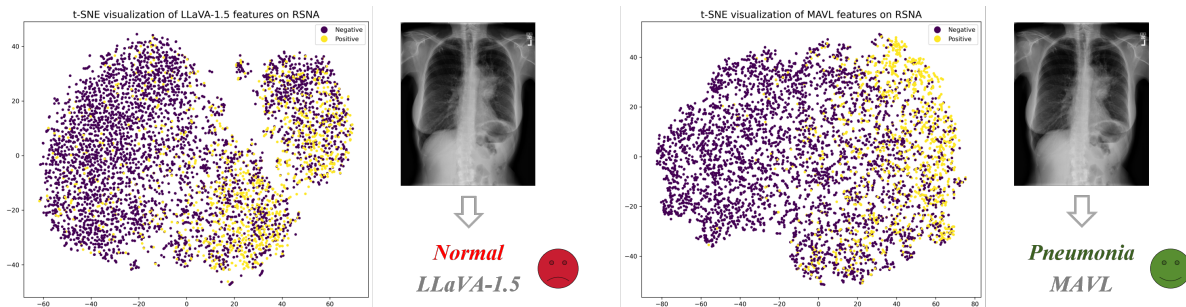


Figure 1. Feature distribution visualization of LLaVA-1.5 (left) and MAVL (right) on the RSNA dataset.

optimal performance in image classification, particularly when dealing with complex medical images. To enhance the generalization capability of MLLMs in radiology disease recognition tasks, we employed a fine-tuning strategy and performed supervised fine-tuning on the MIMIC-CXR dataset [18]. Additionally, inspired by the work of Zhang *et al.* [16], we incorporated a series of optimizations. While these improvements yielded performance gains, the results remained inferior compared to traditional CLIP-based models. This phenomenon raises a critical question: *Can MLLMs effectively perform zero-shot disease recognition?*

To answer the aforementioned question, we visualize the feature distributions of LLaVA and MAVL [8] on the RSNA [19] dataset, as illustrated in Fig. 1. The results indicate that LLaVA exhibits strong feature extraction capabilities, comparable to the well-established MAVL in the domain. However, in the disease recognition task, MAVL significantly outperforms LLaVA. We hypothesize that this performance gap arises because MLLMs fail to fully utilize the extracted features for effective disease identification. To address this limitation, we propose a *simple yet effective* LLaVA-RadZ framework for zero-shot disease recognition. Firstly, we introduce a new end-to-end training strategy, Decoding-Side Feature Alignment Training (DFAT). Specifically, we introduce special tokens for both image and text modalities and leverage the autoregressive generation capability of the decoder architecture to extract global representations of images and texts. Additionally, we incorporate a cross-modal contrastive loss to optimize the model’s ability to learn discriminative features. Furthermore, to mitigate the semantic category gap encountered during fine-grained alignment between medical images and textual reports, we design a Domain Knowledge Anchoring Module (DKAM). DKAM utilizes the model’s intrinsic medical knowledge to extract the semantic information underlying disease categories, constructing disease description vectors that serve as an intermediary bridge to facilitate the alignment between medical images and textual reports, thereby establishing a stable trimodal relationship. To further enhance the correlation among medical images, textual reports, and disease categories, a category knowledge-guided

loss strengthens the association between similar images and corresponding textual reports.

Our main contributions can be summarized as follows.

- We propose a novel end-to-end training strategy, Decoding-Side Feature Alignment Training (DFAT), and incorporate a cross-modal contrastive loss to optimize the model’s ability to achieve effective alignment between visual and textual features.
- We design a Domain Knowledge Anchoring Module (DKAM) to leverage MLLM’s intrinsic medical knowledge and effectively mitigate semantic gap in image-text alignment, thereby enhancing category-level alignment.
- We conduct extensive experiments on multiple large-scale radiology diagnosis datasets, validating the potential of LLaVA-RadZ in zero-shot disease recognition tasks.

2. Related Work

Multi-modal Large Language Models. Inspired by the exceptional reasoning capabilities of large language models (LLMs), researchers are actively exploring ways to extend these abilities to the visual domain, driving advancements in multimodal LLMs. With the release of GPT-4 (Vision) [9] and Gemini [10], these models have demonstrated remarkable multimodal understanding and generation capabilities, further fueling research in this field.

To bridge the gap between vision encoders and LLMs, BLIP-2 [24] introduces a Q-Former that transforms image features into a format compatible with LLMs, enabling seamless integration with text embeddings. LLaVA [11] and MiniGPT-4 [25] further enhance generalization and task performance by leveraging large-scale multimodal pre-training, followed by instruction tuning for specific applications. In the medical domain, LLMs have shown immense potential for advancing research and practical applications. Med-Flamingo [26] extends Flamingo to the medical field by pretraining on multimodal knowledge sources spanning multiple medical disciplines. LLaVA-Med [15] refines image-text pairs from PMC-15M [27] and trains a biomedical-specialized MLLM using a limited dataset, building upon the pre-trained parameters of LLaVA. Similarly, Med-PaLM [28] fine-tunes PaLM [29] using domain-

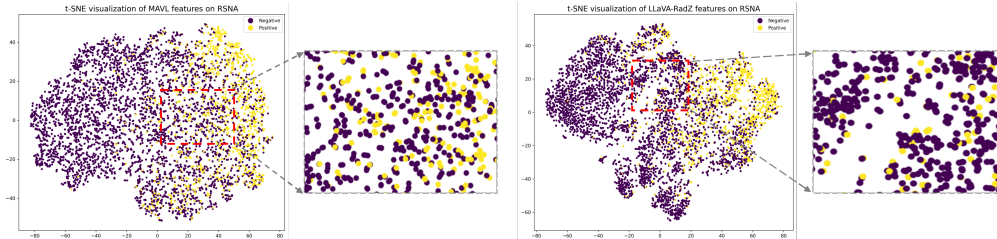


Figure 2. Comparison of Feature Distributions between MAVL and LLaVA-RadZ on the RSNA Dataset.

Table 1. Comparison of zero-shot disease classification performance of public MLLMs and LLaVA-based exploratory methods across five medical benchmarks. “FT” denotes supervised fine-tuning with LoRA, “CoT” refers to zero-shot chain-of-thought prompting templates, and “Inference” represents CLIP inference strategies. The best results are highlighted in bold and the second-best results are underlined.

Dataset		CheXpert [20]			ChestXray-14 [21]			COVIDx CXR-2 [22]			RSNA Pneumonia [19]			SIIM-ACR [23]		
Method	Model	AUC ↑	F1 ↑	ACC ↑	AUC ↑	F1 ↑	ACC ↑	AUC ↑	F1 ↑	ACC ↑	AUC ↑	F1 ↑	ACC ↑	AUC ↑	F1 ↑	ACC ↑
MLLM	LLaVA-1.5 (7B) [11]	-	7.50	8.28	-	3.33	6.92	-	53.14	50.28	-	40.53	55.34	-	23.66	50.36
	LLaVA-Med (7B) [15]	-	6.87	8.94	-	8.02	6.78	-	34.90	50.03	-	18.58	50.00	-	21.91	49.90
	Qwen2.5-Max [12]	-	32.23	67.97	-	19.04	76.19	-	<u>75.91</u>	<u>76.81</u>	-	43.58	43.59	-	64.70	<u>72.57</u>
	Gemini-Pro [10]	-	35.01	76.08	-	14.16	77.78	-	62.84	62.90	-	44.23	51.43	-	61.43	72.03
	GPT-4o [9]	-	<u>45.85</u>	<u>81.14</u>	-	19.85	<u>81.55</u>	-	50.93	77.08	-	54.20	65.33	-	64.57	72.11
Explorative Methods	LLaVA-1.5-7B _{FT}	-	10.61	19.62	-	7.85	19.06	-	27.74	25.18	-	43.60	34.80	-	52.37	50.95
	LLaVA-Med-7B _{FT}	-	14.25	31.46	-	9.00	21.43	-	27.42	24.09	-	46.72	38.88	-	53.11	57.68
	LLaVA-Med-7B _{FT} + CoT [16]	-	8.90	26.23	-	8.33	20.46	-	27.12	26.55	-	49.59	43.80	-	54.06	51.07
	LLaVA-Med-7B _{FT} + Inference [16]	71.00	44.85	75.45	64.30	<u>21.73</u>	70.86	71.07	69.84	60.39	77.51	<u>69.85</u>	<u>72.90</u>	71.25	<u>68.26</u>	71.27
	Ours	LLaVA-RadZ _{FT}	75.63	48.41	81.77	70.75	27.86	84.57	81.76	76.65	74.41	85.94	75.84	81.35	86.32	76.89

specific medical instructions, demonstrating strong performance under human evaluation frameworks. Other notable models, such as Chat-Doctor [30] and Med-Alpaca [31], have been tailored for medical question-answering and dialogue applications.

Despite the significant progress of MLLMs, several challenges remain [16, 32–34]. Recent studies [16, 34] highlight the suboptimal performance of MLLMs in image classification, particularly in fine-grained category recognition. We find that this issue is especially pronounced in the medical domain, where precise classification is crucial for medical applications. To address these shortcomings, we are refining traditional MLLM training paradigms to enhance classification performance and improve fine-grained category comprehension.

Prompt Engineering. Prompting enhances the ability of pre-trained large language models (LLMs) to understand tasks by incorporating language instructions into the input text [35–38]. Recently, prompt-based techniques have also been applied to vision-language models to improve performance. In medical vision-language models (VLMs), GLORIA [39] generates a set of textual prompts to describe potential subtypes, severity levels, and anatomical locations for each disease category. MedKLIP [6] enhances model performance by retrieving descriptions of medical entities from the UMLS knowledge base [40]. CARZero [5] introduces a prompt-alignment strategy based on LLMs, integrating prompt templates into the training dataset to ensure alignment during both training and inference. MAVL [8] uses visual descriptions of pathological features to guide the

model in effectively detecting diseases in medical images.

Although these approaches have successfully improved model performance through prompt-based strategies, they all rely on external models or expert knowledge, without fully leveraging the model’s intrinsic understanding capabilities. Fortunately, recent research on LLaVA-Med [15] has demonstrated remarkable domain-specific conversational abilities, proving that it possesses a certain level of medical knowledge. Building upon LLaVA-Med [15], we further explore the feasibility of utilizing the model’s inherent comprehension to enhance zero-shot medical classification performance.

3. Approach

3.1. Can Med-LLMs Be Good Medical Classifiers?

Previous studies have explored the classification capabilities of multimodal large language models (MLLMs), revealing that their performance on image classification tasks is often limited. For example, Zhang *et al.* [16] investigates the performance differences in classification between MLLMs and CLIP, focusing on factors such as inference strategies, training approaches, and datasets. Inspired by this work, we extend the exploration to zero-shot tasks in the medical domain. Unlike natural images and text, the relationship between medical images and reports is more complex. We seek to investigate whether large medical models, leveraging domain-specific knowledge, can achieve superior performance on medical zero-shot tasks.

We first evaluated two open-source MLLMs, *i.e.*, LLaVA-1.5 [11] and LLaVA-Med [15], on five medical

datasets in a zero-shot classification setting. The evaluation followed a general large-model classification approach, where the model selects the correct category from a set of candidate options. As shown in Tab. 1, these models demonstrated limited performance in disease classification tasks and failed to accurately identify various medical conditions. Given the potential knowledge limitations of these models, we further assessed the performance of more powerful proprietary MLLMs (*i.e.*, Qwen2.5-Max [12], Gemini-Pro [10], and GPT-4o [9]) on zero-shot medical disease recognition tasks. As shown in Tab. 1, these models exhibited superior classification capabilities. However, they still lagged behind the state-of-the-art domain-specific methods in medical classification.

To enhance the generalization ability of MLLMs in radiology disease identification, we conducted Supervised Fine-Tuning (SFT) on LLaVA-1.5 [11] and LLaVA-Med [15] using the publicly available MIMIC-CXR dataset [18]. Surprisingly, the fine-tuned models did not achieve consistent performance improvements across the five datasets. In some cases, their classification performance even deteriorated. Further analysis of the model outputs revealed that MLLMs did not always focus on disease-specific information in radiology reports. Instead, they tended to overlearn the textual structures and linguistic patterns of the reports, which limited their classification capability. To mitigate this issue, we incorporated the Chain-of-Thought (CoT) prompting strategy and adjusted the model’s reasoning approach, inspired by the methodology of Zhang *et al.* [16], to optimize the model’s decision-making process. This approach led to moderate improvements in classification performance on medical datasets. Although the models have not yet reached optimal performance, the results suggest that MLLMs still hold significant potential for zero-shot medical disease recognition.

3.2. Motivation

As previously discussed, despite possessing a certain level of domain knowledge, medical MLLMs have not yet demonstrated remarkable performance in zero-shot medical tasks. Even with further instruction tuning, their performance remains inferior to that of existing vision-language models (VLMs). However, it is noteworthy that modifying the inference strategy leads to significant performance improvements, suggesting that MLLMs are indeed capable of capturing medical image and text features. Nevertheless, these features have yet to be fully exploited.

To address this limitation, we propose the LLaVA-RadZ framework, introducing a novel end-to-end training strategy, Decoding-Side Feature Alignment Training (DFAT). This approach leverages the unique properties of the MLLM decoder architecture while incorporating modality-specific special tokens to facilitate effective interaction between

medical images and textual features, ultimately achieving more robust cross-modal alignment. As illustrated in Fig. 2, we compare the feature distribution of our model with MAVL [8], the current state-of-the-art method, on the RSNA [19] dataset. The results clearly demonstrate that our model achieves better clustering of intra-class samples while enhancing inter-class separation, validating the effectiveness of our approach. Furthermore, we introduce the Domain Knowledge Anchor Module (DKAM), which harnesses the intrinsic medical knowledge of LLMs to bridge the semantic gap between images and text, enabling more precise disease classification.

3.3. The Proposed LLaVA-RadZ

We aim to learn generalizable medical image representations from radiology reports to enhance various downstream medical image recognition tasks, particularly when labeled data is scarce. The overall framework is illustrated in Fig. 3. Given a pair of medical images and reports, the image and text are first passed through separate visual and text encoders to obtain their respective encoded features. These encoded features and specially designed tokens are then fed into a language model to obtain the final feature representation. The features are mapped into a common representational space via an MLP projection layer and optimized with the InfoNCE loss. Furthermore, we propose a Domain Knowledge Anchor Module (DKAM), which leverages domain knowledge inherent in the model to guide the alignment of text and image features at the category level.

3.3.1. End-to-End Training Strategy

Currently, most MLLMs employ generation-based training objectives for instruction fine-tuning. Although this approach effectively captures the features of medical images and textual reports, its performance in zero-shot tasks remains suboptimal, as it fails to fully leverage these features. To address this issue, we propose a novel training strategy, Decoding-Side Feature Alignment Training (DFAT), as illustrated in Fig. 3.

We consider a training dataset consisting of N pairs of medical image-text samples, denoted as $S_{\text{train}} = \{(X_1, Y_1), \dots, (X_N, Y_N)\}$. The medical image $X_i \in \mathbb{R}^{H \times W \times 3}$, with H and W representing the height and width of the image, respectively. Y_i refers to the corresponding medical text report associated with the image.

Specifically, we design special tokens for both image and text modalities, where $\langle \text{ImgCls}_i \rangle (i = 0, \dots, 4)$ denotes image feature tokens and $\langle \text{TxtCls}_i \rangle (i = 0, \dots, 8)$ denotes text feature tokens. These special tokens are attached to the image prompt X_{prompt} and the text prompt Y_{prompt} , respectively. The image prompt X_{prompt} has a format similar to “What disease is indicated by the chest X-ray?”, while the text prompt Y_{prompt} follows a format such as “What disease

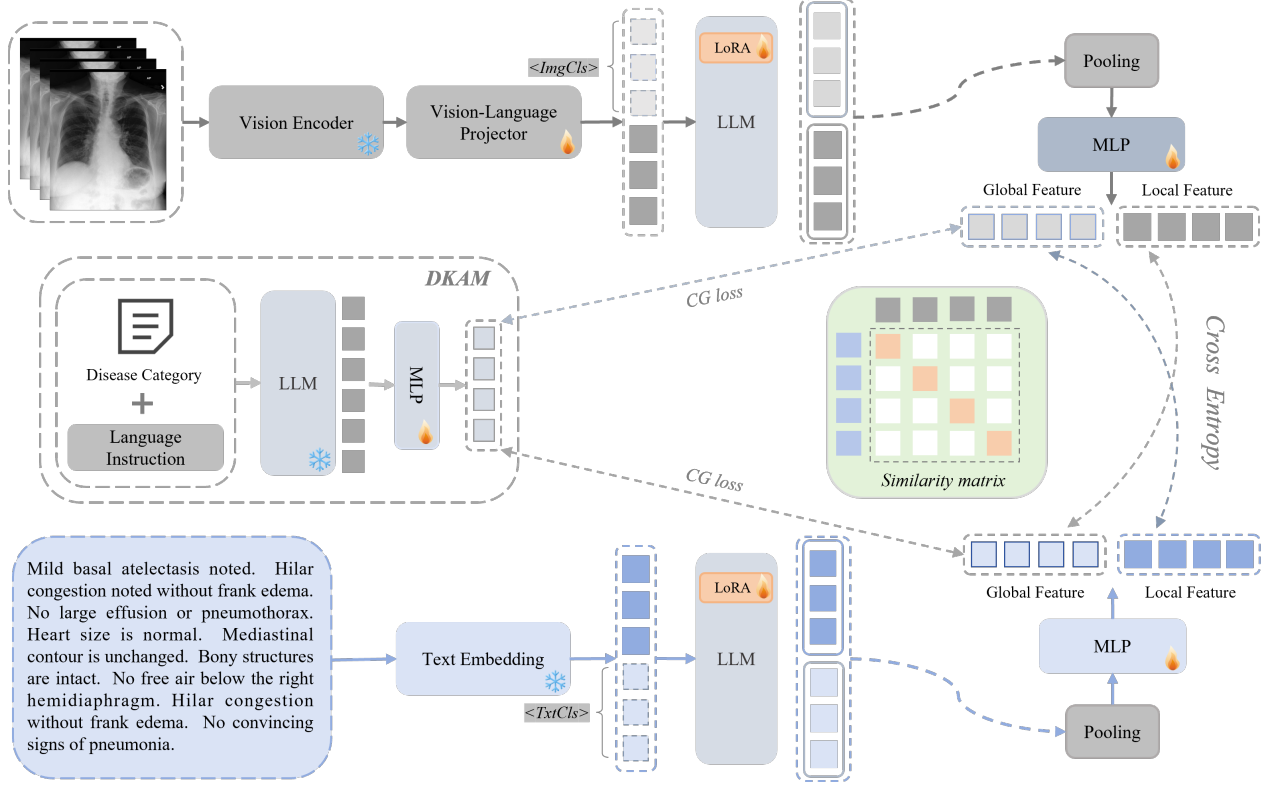


Figure 3. The LLaVA-RadZ framework consists of three components. (A) Construct a category semantic vector repository using the domain knowledge anchoring module (DKAM). (B) Encode medical images and text, appending $\langle \text{ImgCls} \rangle$ and $\langle \text{TxtCls} \rangle$ tokens before feeding them into the LLM. (C) Extract global and local features, optimizing with cross-entropy loss, while leveraging the semantic repository for category-level alignment.

is described in this text?”. By appending special tokens, we obtain the modified prompts $\tilde{X}_{\text{prompt}}$ and $\tilde{Y}_{\text{prompt}}$, which is represented as:

$$\tilde{X}_{\text{prompt}} = X_{\text{prompt}} + \langle \text{ImgCls}_i \rangle_{(i=0, \dots, 4)}, \quad (1)$$

$$\tilde{Y}_{\text{prompt}} = Y_{\text{prompt}} + \langle \text{TxtCls}_i \rangle_{(i=0, \dots, 8)}. \quad (2)$$

When an image and its corresponding prompt $\tilde{X}_{\text{prompt}}$ are input into the MLLM \mathcal{F} to generate a response \hat{R}_{img} . Similarly, when a text sample and its corresponding feature extraction prompt $\tilde{Y}_{\text{prompt}}$ are provided as input, the model produces a response \hat{R}_{txt} . This process can be formally expressed as:

$$\hat{R}_{\text{img}}^i = \mathcal{F}(X_i, \tilde{X}_{\text{prompt}}), \quad \hat{R}_{\text{txt}}^i = \mathcal{F}(Y_i, \tilde{Y}_{\text{prompt}}). \quad (3)$$

Due to the autoregressive nature of the decoder architecture, when the LLM processes visual and textual information to generate responses, its internal representations are stored in the designated special tokens. Specifically, we extract the penultimate layer embedding \tilde{h}_{img} corresponding to the special token $\langle \text{ImgCls}_i \rangle$, which stores the global image features $H_{\text{img}}^{\text{global}} \in \mathbb{R}^{B \times I \times K}$. Here, B denotes the

number of image-text pairs in each batch, I represents the number of special image tokens, and K is the dimension of the shared embedding space. After applying a pooling operation followed by an MLP projection layer γ_{img} , we obtain the global image feature representation $X_g \in \mathbb{R}^{B \times K}$. The local image feature $X_l \in \mathbb{R}^{B \times K}$ is obtained by pooling the hidden states of all tokens except those corresponding to special tokens, followed by an MLP projection layer γ_{img} :

$$\begin{aligned} X_g &= \gamma_{\text{img}}(\text{AvgPool}(H_{\text{img}}^{\text{global}})), \\ X_l &= \gamma_{\text{img}}(\text{AvgPool}(H_{\text{img}}^{\text{local}})). \end{aligned} \quad (4)$$

Similarly, we extract the global text representation $Y_g \in \mathbb{R}^{B \times K}$ and the local text representation $Y_l \in \mathbb{R}^{B \times K}$ using the same methodology:

$$\begin{aligned} Y_g &= \gamma_{\text{txt}}(\text{AvgPool}(H_{\text{txt}}^{\text{global}})), \\ Y_l &= \gamma_{\text{txt}}(\text{AvgPool}(H_{\text{txt}}^{\text{local}})). \end{aligned} \quad (5)$$

To further enhance fine-grained alignment across different modalities, we introduce a cross-modal contrastive loss, L_{CA} . Specifically, for the i -th image-text pair (X_i, Y_i) in a batch, we alternately align the global and local fea-

tures of images and texts. This procedure yields two symmetric, temperature-normalized InfoNCE objectives: one aligns global image features with local text features, and the other aligns local image features with global text features. These objectives maximize the mutual information between image-text pairs in the latent space.

For the alignment between global image features and local text features, we calculate two similarity matrices, $S_i^{X_g \rightarrow Y_l}$ and $S_i^{Y_l \rightarrow X_g}$, with the following computation:

$$S_i^{X_g \rightarrow Y_l} = \frac{X_{g,i} \cdot Y_{l,i}^T}{\tau}, \quad S_i^{Y_l \rightarrow X_g} = \frac{Y_{l,i} \cdot X_{g,i}^T}{\tau}. \quad (6)$$

where τ is the temperature hyperparameter. Subsequently, we compute the contrastive loss between the global image and the local text, with the following formula:

$$\begin{aligned} L_{CA}^{X_g \rightarrow Y_l, i} &= -\log \frac{\exp(S_i^{X_g \rightarrow Y_l})}{\sum_{k=1}^B \exp(S_k^{X_g \rightarrow Y_l})}, \\ L_{CA}^{Y_l \rightarrow X_g, i} &= -\log \frac{\exp(S_i^{Y_l \rightarrow X_g})}{\sum_{k=1}^B \exp(S_k^{Y_l \rightarrow X_g})}, \\ L_{CA}^{X_g \rightarrow Y_l} &= \frac{1}{2} \sum_{i=1}^B (L_{CA}^{X_g \rightarrow Y_l, i} + L_{CA}^{Y_l \rightarrow X_g, i}). \end{aligned} \quad (7)$$

Similarly, for the alignment between local image features and global text features, we compute the contrastive loss between the local image and global text.

$$\begin{aligned} L_{CA}^{X_l \rightarrow Y_g} &= -\frac{1}{2} \sum_{i=1}^B \left(\log \frac{\exp(S_i^{X_l \rightarrow Y_g})}{\sum_{k=1}^B \exp(S_k^{X_l \rightarrow Y_g})} \right. \\ &\quad \left. + \log \frac{\exp(S_i^{Y_g \rightarrow X_l})}{\sum_{k=1}^B \exp(S_k^{Y_g \rightarrow X_l})} \right). \end{aligned} \quad (8)$$

Finally, we obtain our cross-modal contrastive loss L_{CA} .

$$L_{CA} = \frac{1}{2} (L_{CA}^{X_g \rightarrow Y_l} + L_{CA}^{X_l \rightarrow Y_g}). \quad (9)$$

3.3.2. Domain Knowledge Anchor Module

In aligning medical images with text reports, we observed that the critical entity of the medical disease categories was merely encoded as features by the model, without considering the underlying semantics. To address this limitation and further enhance fine-grained alignment capabilities, we introduce the Domain Knowledge Anchoring Module (DKAM). Initially, we leverage the inherent medical domain expertise of an LLM to generate descriptive explanations for each disease category. These generated disease descriptions serve as an intermediary bridge to guide the alignment between medical images and text reports. Specifically, we input the disease list D_{list} from the training dataset along

with a designed prompt template K_{prompt} into the LLM \mathcal{F} . This process is formally expressed as:

$$\hat{R}_{\text{dis}} = \mathcal{F}(D_{\text{list}}, K_{\text{prompt}}). \quad (10)$$

By fully harnessing the LLM’s exceptional semantic understanding, we prompt the model to explore the underlying semantics of the disease categories and discern their distinctions, ultimately producing a refined disease description. The features extracted from the LLM’s response are then mapped via a multi-layer perceptron (MLP) to yield the disease description vector \hat{D} , which is represented as:

$$\hat{D} = \gamma_{\text{dis}} (\hat{R}_{\text{dis}}). \quad (11)$$

Subsequently, we introduce the Category of Knowledge-guided Contrastive Loss L_{CG} . Specifically, we calculate the cross-entropy loss between the disease description vector \hat{D} and the global features of both the images X_g and the text Y_g . This design encourages the model to better capture the semantic relationships among images, text, and disease categories during training, achieving a more robust category-level alignment.

$$S_i^{\text{img-disease}} = \frac{X_{g,i} \cdot \hat{D}^T}{\tau}, \quad S_i^{\text{txt-disease}} = \frac{Y_{g,i} \cdot \hat{D}^T}{\tau}. \quad (12)$$

$$\begin{aligned} L_{CG, i}^{\text{txt}} &= -\log \frac{\exp(S_i^{\text{txt-disease}})}{\sum_{k=1}^N \exp(S_k^{\text{txt-disease}})}, \\ L_{CG, i}^{\text{img}} &= -\log \frac{\exp(S_i^{\text{img-disease}})}{\sum_{k=1}^N \exp(S_k^{\text{img-disease}})}. \end{aligned} \quad (13)$$

Here, N represents the number of disease categories, B denotes the number of medical image-text pairs in each batch, and τ is the temperature hyperparameter. The final category of knowledge-guided loss is as follows:

$$L_{CG} = \frac{1}{2} \sum_{i=1}^B (L_{CG, i}^{\text{txt}} + L_{CG, i}^{\text{img}}). \quad (14)$$

By combining the category knowledge-guided loss and the cross-modal contrastive loss, the final objective function is defined as follows:

$$L_{\text{total}} = \lambda L_{CA} + (1 - \lambda) L_{CG}, \quad (15)$$

where λ is a balancing factor used to adjust the weights of the two losses, and it is set to 0.5 by default.

4. Experiments

In this section, we first provide an overview of the dataset employed in our experiments, including those used for pre-training and the various downstream tasks. Subsequently, we outline the implementation details and describe the baselines considered for comparison.

Table 2. Comparison of performance with other SOTA methods on four medical datasets for the zero-shot classification task, with AUC, F1, and ACC scores reported. The best results are highlighted in bold and the second-best results are underlined.

Dataset	ChestXray-14 [21]			COVIDx CXR-2 [22]			RSNA Pneumonia [19]			SIIM-ACR [23]		
	AUC ↑	F1 ↑	ACC ↑	AUC ↑	F1 ↑	ACC ↑	AUC ↑	F1 ↑	ACC ↑	AUC ↑	F1 ↑	ACC ↑
ConVIRT [41]	53.15	12.38	57.88	62.78	71.23	63.84	79.21	55.67	75.08	64.25	42.87	53.42
GLoRIA [39]	55.92	14.20	59.47	64.52	70.78	60.21	70.37	48.19	70.54	54.71	40.39	47.15
BioViL [42]	57.82	15.64	61.33	61.40	70.92	58.20	84.12	54.59	74.43	70.28	46.45	68.22
CheXzero [43]	66.99	21.99	65.38	73.13	76.13	71.45	85.13	61.49	78.34	84.60	65.97	77.34
MedKLIP [6]	<u>72.33</u>	24.18	79.40	76.28	76.54	71.96	<u>86.57</u>	63.28	79.97	<u>89.79</u>	72.73	<u>83.99</u>
MAVL [8]	73.50	<u>26.25</u>	<u>82.77</u>	83.86	81.73	78.07	86.91	<u>63.41</u>	82.42	92.04	77.95	87.14
Ours	70.75	27.86	84.57	<u>81.76</u>	<u>76.65</u>	<u>74.41</u>	85.94	75.84	<u>81.35</u>	86.32	<u>76.89</u>	79.28

Table 3. Comparison of performance with other SOTA methods at different data portions for fine-tuning classification task. AUC scores are reported. The best results are highlighted in bold and the second-best results are underlined.

Dataset	RSNA Pneumonia [19]			Pneumothorax [23]			COVIDx CXR-2 [22]		
	1%	10%	100%	1%	10%	100%	1%	10%	100%
Scratch	68.94	83.31	87.12	53.11	76.18	87.48	85.11	93.65	98.86
ConVIRT [41]	78.86	85.42	87.64	72.39	80.41	91.67	90.30	97.74	99.70
GLoRIA [39]	79.13	85.59	87.83	75.85	86.20	91.89	92.74	97.18	99.54
BioViL [42]	80.27	86.04	88.29	70.29	79.45	88.05	92.39	98.39	99.68
MedKLIP [6]	82.11	87.14	88.58	85.24	<u>89.91</u>	93.02	95.58	98.77	99.77
MAVL [8]	<u>86.09</u>	<u>87.90</u>	<u>88.94</u>	91.53	93.00	94.48	<u>97.18</u>	<u>99.15</u>	<u>99.90</u>
Ours	88.12	88.45	89.29	<u>88.07</u>	89.85	<u>94.27</u>	98.34	99.81	99.97

4.1. Dataset

In our experiments, we pre-trained the model using the MIMIC-CXR dataset [18]. For downstream tasks, we primarily evaluated the model’s performance in medical disease classification using multiple benchmark datasets, including ChestX-ray14 [21], RSNA Pneumonia [19], SIIM-ACR Pneumothorax [23], CheXpert [20], and COVIDx CXR-2 [22]. Detailed information on these datasets can be found in the supplementary material.

4.2. Evaluation Metrics

For the zero-shot classification task, we employ standard classification evaluation metrics, including Accuracy, AUC score, and F1 score. The macro-average metrics are reported for all diseases present in the target dataset.

4.3. Zero-shot evaluation

As shown in Tab. 2, we compare the performance of established methods in the field on the zero-shot classification task for radiological diseases, evaluated on four officially released test datasets. Our findings demonstrate that, compared to conventional CLIP-style models such as ConVIRT [41], GLoRIA [39], BioViL [42], and CheXzero [43], our approach exhibits significant advantages. Even when compared to state-of-the-art models incorporating external

models or domain-specific expert knowledge, our method remains highly competitive. Specifically, on the multi-class dataset ChestXray-14, our model surpasses the supervised learning method MAVL [8] by 1.8% in accuracy. Moreover, on the RSNA Pneumonia dataset, we achieve a 12.43% improvement in F1 score. These results indicate that multi-modal large language models (MLLMs) possess strong feature extraction capabilities, further underscoring their immense potential in medical disease classification tasks.

4.4. Fine-tuning evaluation

Consistent with previous studies [6, 8], we fine-tune the model on downstream datasets using 1%, 10%, and 100% of the available data and further evaluate its performance. Tab. 3 presents the fine-tuning results across three datasets, demonstrating that our model consistently maintains a competitive advantage. Notably, when fine-tuned with only 1% data, our proposed LLaVA-RadZ outperforms the MAVL [8] model by 2.03% on the RSNA Pneumonia and by 1.16% on COVIDx. Even when fine-tuned with 100% data, our model continues to deliver performance improvements. This enhancement is likely attributed to our decoder-side alignment training strategy, which effectively captures global modality information and leverages the interaction between global and local features to achieve fine-grained

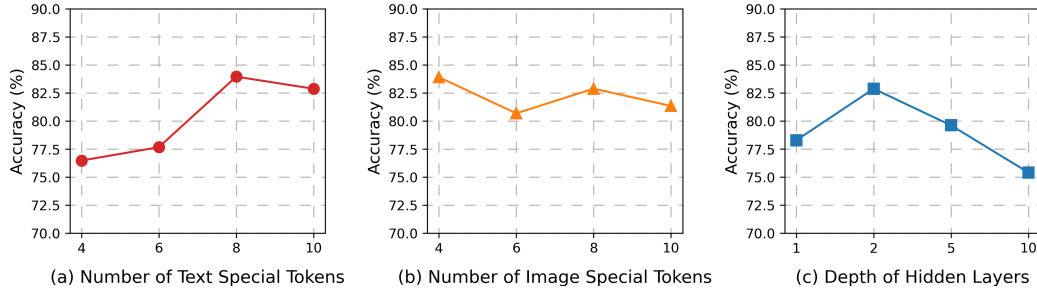


Figure 4. Effect of Special Token Numbers and Hidden Layer Depth on ChestXray-14 Classification.

Table 4. Ablation study of DKAM on ChestXray-14. D_1 represents a semantic vector library of 75 medical entities, and D_2 represents a semantic vector library of 14 disease categories.

#	DKAM	D_1	D_2	AUC \uparrow	F1 \uparrow	ACC \uparrow
a				69.11	27.25	82.63
b	✓	✓		68.61	25.47	81.61
c	✓		✓	70.75	27.86	84.57

cross-modal alignment, further strengthening the model’s disease recognition capability.

4.5. Ablation Study

Ablation Study of DKAM. To validate the effectiveness of our proposed Domain Knowledge Anchor Module (DKAM), we conducted an ablation study on the ChestXray-14 dataset. With DKAM incorporated, we further investigated the impact of different category semantic vector repositories on the model’s fine-grained alignment capability. Consistent with the previous MedKLIP study, we selected 75 primary medical entities from the MIMIC-CXR dataset. However, unlike MedKLIP, we leveraged the model’s intrinsic domain knowledge to construct a category semantic vector repository, denoted as D_1 . Additionally, we built a disease-specific semantic vector repository for the 14 medical disease categories present in the MIMIC-CXR training dataset, denoted as D_2 .

As shown in Tab. 4 (a vs. c), the introduction of DKAM significantly enhances model performance. Using disease category semantics as an intermediary facilitates more precise alignment between medical images and textual descriptions at the category level. Further comparisons in Tab. 4 (b vs. c) demonstrate that, compared to a larger repository of medical entities, a semantic vector repository focusing on primary disease categories provides stronger guidance for image-text alignment. Moreover, additional medical entities in D_1 , such as tip, tube, PICC, and device, may introduce noise and negatively impact alignment at the disease category level. This adverse effect is corroborated by the comparative results in Tab. 4 (a vs. b).

Ablation Study of Special Tokens. As shown in Tab. 1, we have demonstrated the effectiveness of the Decoding-Side

Table 5. Ablation study of feature representations on ChestXray-14.

#	Global	Local	Prompt	AUC \uparrow	F1 \uparrow	ACC \uparrow
a		✓		67.14	25.08	77.88
b		✓	✓	68.19	26.33	78.76
c	✓		✓	69.28	26.13	82.48
d	✓	✓	✓	70.75	27.86	84.57

Feature Alignment Training (DFAT) strategy. To further investigate the design of the critical special tokens integral to this approach, we conducted an in-depth analysis on the ChestXray-14 dataset. As illustrated in Fig. 4, we observed that the number of text and image tokens significantly influences model performance, with both an excessive and an insufficient count potentially resulting in a loss of modal information. Moreover, our study indicates that the optimal global features are not stored in the final hidden layer but rather in the penultimate layer, which may be attributed to the loss of fine-grained information due to deeper feature aggregation, thereby affecting overall performance.

Ablation Study of Features. During the process of cross-modal alignment, we conducted a detailed analysis of the impact of global and local features on model performance, and further investigated the effectiveness of using prompts, as shown in Tab. 5. The experimental results indicate that utilizing only local features yields the poorest performance, while relying solely on global features provides a certain advantage over local features. This may be attributed to the fact that the specially designed tokens for each modality can more precisely capture the global information of the corresponding modality. Moreover, the combination of global and local features achieves the best performance. Additionally, the incorporation of prompts further enhances the model’s ability to capture feature information.

5. Conclusion

This paper proposes a simple yet effective framework, LLaVA-RadZ, for zero-shot medical disease recognition. First, we introduce an end-to-end decoding-side feature alignment training strategy to leverage the characteristics of the MLLM architecture and effectively store modality-

related information. Additionally, we employ cross-modal contrastive learning to optimize feature alignment across modalities, enhancing the model’s cross-modal understanding capabilities. Furthermore, we propose a domain knowledge anchoring Module to facilitate category-level alignment between medical images and textual descriptions. Experimental results demonstrate that LLaVA-RadZ achieves outstanding performance across multiple benchmarks, highlighting the significant potential of MLLMs in tackling zero-shot radiological disease recognition tasks.

References

- [1] Heang-Ping Chan, Lubomir M Hadjiiski, and Ravi K Samala. Computer-aided diagnosis in the era of deep learning. *Medical physics*, 47(5):e218–e227, 2020. 1
- [2] Mohammad Jamshidi, Ali Lalbakhsh, Jakub Talla, Zdeněk Peroutka, Farimah Hadjiiooei, Pedram Lalbakhsh, Morteza Jamshidi, Luigi La Spada, Mirhamed Mirmozafari, Mojgan Dehghani, et al. Artificial intelligence and covid-19: deep learning approaches for diagnosis and treatment. *Ieee Access*, 8:109581–109595, 2020.
- [3] Junghwan Lee, Cong Liu, Junyoung Kim, Zhehuan Chen, Yingcheng Sun, James R Rogers, Wendy K Chung, and Chunhua Weng. Deep learning for rare disease: A scoping review. *Journal of biomedical informatics*, 135:104227, 2022.
- [4] Khoa A Tran, Olga Kondrashova, Andrew Bradley, Elizabeth D Williams, John V Pearson, and Nicola Waddell. Deep learning in cancer diagnosis, prognosis and treatment selection. *Genome medicine*, 13:1–17, 2021. 1
- [5] Haoran Lai, Qingsong Yao, Zihang Jiang, Rongsheng Wang, Zhiyang He, Xiaodong Tao, and S Kevin Zhou. Carzero: Cross-attention alignment for radiology zero-shot classification. In *Proceedings of the IEEE/CVF Conference on Computer Vision and Pattern Recognition*, pages 11137–11146, 2024. 1, 3
- [6] Chaoyi Wu, Xiaoman Zhang, Ya Zhang, Yanfeng Wang, and Weidi Xie. Medklip: Medical knowledge enhanced language-image pre-training for x-ray diagnosis. In *Proceedings of the IEEE/CVF International Conference on Computer Vision*, pages 21372–21383, 2023. 1, 3, 7
- [7] Xiaoman Zhang, Chaoyi Wu, Ya Zhang, Weidi Xie, and Yanfeng Wang. Knowledge-enhanced visual-language pre-training on chest radiology images. *Nature Communications*, 14(1):4542, 2023. 1
- [8] Vu Minh Hieu Phan, Yutong Xie, Yuankai Qi, Lingqiao Liu, Liyang Liu, Bowen Zhang, Zhibin Liao, Qi Wu, Minh-Son To, and Johan W Verjans. Decomposing disease descriptions for enhanced pathology detection: A multi-aspect vision-language pre-training framework. In *Proceedings of the IEEE/CVF Conference on Computer Vision and Pattern Recognition*, pages 11492–11501, 2024. 1, 2, 3, 4, 7
- [9] Josh Achiam, Steven Adler, Sandhini Agarwal, Lama Ahmad, Ilge Akkaya, Florencia Leoni Aleman, Diogo Almeida, Janko Altmenschmidt, Sam Altman, Shyamal Anadkat, et al. Gpt-4 technical report. *arXiv preprint arXiv:2303.08774*, 2023. 1, 2, 3, 4
- [10] Gemini Team, Rohan Anil, Sebastian Borgeaud, Jean-Baptiste Alayrac, Jiahui Yu, Radu Soricut, Johan Schalkwyk, Andrew M Dai, Anja Hauth, Katie Millican, et al. Gemini: a family of highly capable multimodal models. *arXiv preprint arXiv:2312.11805*, 2023. 2, 3, 4
- [11] Haotian Liu, Chunyuan Li, Qingyang Wu, and Yong Jae Lee. Visual instruction tuning. *Advances in neural information processing systems*, 36:34892–34916, 2023. 1, 2, 3, 4
- [12] An Yang, Baosong Yang, Beichen Zhang, Binyuan Hui, Bo Zheng, Bowen Yu, Chengyuan Li, Dayiheng Liu, Fei Huang, Haoran Wei, et al. Qwen2. 5 technical report. *arXiv preprint arXiv:2412.15115*, 2024. 3, 4
- [13] Wenxuan Huang, Zijie Zhai, Yunhang Shen, Shaoshen Cao, Fei Zhao, Xiangfeng Xu, Zheyu Ye, and Shaohui Lin. Dynamic-llava: Efficient multimodal large language models via dynamic vision-language context sparsification. *arXiv preprint arXiv:2412.00876*, 2024.
- [14] Shengqiong Wu, Hao Fei, Leigang Qu, Wei Ji, and Tat-Seng Chua. Next-gpt: Any-to-any multimodal llm. In *Forty-first International Conference on Machine Learning*, 2024. 1
- [15] Chunyuan Li, Cliff Wong, Sheng Zhang, Naoto Usuyama, Haotian Liu, Jianwei Yang, Tristan Naumann, Hoifung Poon, and Jianfeng Gao. Llava-med: Training a large language-and-vision assistant for biomedicine in one day. *Advances in Neural Information Processing Systems*, 36, 2024. 1, 2, 3, 4
- [16] Yuhui Zhang, Alyssa Unell, Xiaohan Wang, Dhruva Ghosh, Yuchang Su, Ludwig Schmidt, and Serena Yeung-Levy. Why are visually-grounded language models bad at image classification? *The Thirty-eighth Annual Conference on Neural Information Processing Systems*, 2024. 1, 2, 3, 4
- [17] Alec Radford, Jong Wook Kim, Chris Hallacy, Aditya Ramesh, Gabriel Goh, Sandhini Agarwal, Girish Sastry, Amanda Askell, Pamela Mishkin, Jack Clark, et al. Learning transferable visual models from natural language supervision. In *International conference on machine learning*, pages 8748–8763. PmLR, 2021. 1
- [18] Alistair EW Johnson, Tom J Pollard, Seth J Berkowitz, Nathaniel R Greenbaum, Matthew P Lungren, Chih-ying Deng, Roger G Mark, and Steven Horng. MIMIC-CXR, a de-identified publicly available database of chest radiographs with free-text reports. *Scientific data*, 6(1):317, 2019. 2, 4, 7
- [19] George Shih, Carol C Wu, Safwan S Halabi, Marc D Kohli, Luciano M Prevedello, Tessa S Cook, Arjun Sharma, Judith K Amorosa, Veronica Arteaga, Maya Galperin-Aizenberg, et al. Augmenting the national institutes of health chest radiograph dataset with expert annotations of possible pneumonia. *Radiology: Artificial Intelligence*, 1(1):e180041, 2019. 2, 3, 4, 7
- [20] Jeremy Irvin, Pranav Rajpurkar, Michael Ko, Yifan Yu, Silvana Ciurea-Ilcus, Chris Chute, Henrik Marklund, Behzad Haghgoo, Robyn Ball, Katie Shpanskaya, et al. Chexpert: A large chest radiograph dataset with uncertainty labels and expert comparison. In *Proceedings of the AAAI conference on artificial intelligence*, volume 33, pages 590–597, 2019. 3, 7

- [21] Xiaosong Wang, Yifan Peng, Le Lu, Zhiyong Lu, Mohammadhadi Bagheri, and Ronald M Summers. Chestx-ray8: Hospital-scale chest x-ray database and benchmarks on weakly-supervised classification and localization of common thorax diseases. In *Proceedings of the IEEE conference on computer vision and pattern recognition*, pages 2097–2106, 2017. 3, 7
- [22] Maya Pavlova, Naomi Terhlan, Audrey G Chung, Andy Zhao, Siddharth Surana, Hossein Aboutalebi, Hayden Gunraj, Ali Sabri, Amer Alaref, and Alexander Wong. Covid-net cxr-2: An enhanced deep convolutional neural network design for detection of covid-19 cases from chest x-ray images. *Frontiers in Medicine*, 9:861680, 2022. 3, 7
- [23] Society for imaging informatics in medicine: Siim-acr pneumothorax segmentation. <https://www.kaggle.com/c/siim-acr-pneumothorax-segmentation>, 2019. 3, 7
- [24] Junnan Li, Dongxu Li, Silvio Savarese, and Steven Hoi. Blip-2: Bootstrapping language-image pre-training with frozen image encoders and large language models. In *International conference on machine learning*, pages 19730–19742. PMLR, 2023. 2
- [25] Deyao Zhu, Jun Chen, Xiaoqian Shen, Xiang Li, and Mohamed Elhoseiny. Minigt-4: Enhancing vision-language understanding with advanced large language models. *arXiv preprint arXiv:2304.10592*, 2023. 2
- [26] Michael Moor, Qian Huang, Shirley Wu, Michihiro Yasunaga, Yash Dalmia, Jure Leskovec, Cyril Zalka, Eduardo Pontes Reis, and Pranav Rajpurkar. Med-flamingo: a multimodal medical few-shot learner. In *Machine Learning for Health (ML4H)*, pages 353–367. PMLR, 2023. 2
- [27] Sheng Zhang, Yanbo Xu, Naoto Usuyama, Jaspreet Bagga, Robert Tinn, Sam Preston, Rajesh Rao, Mu Wei, Naveen Valluri, Cliff Wong, et al. Large-scale domain-specific pre-training for biomedical vision-language processing. *arXiv preprint arXiv:2303.00915*, 2(3):6, 2023. 2
- [28] Karan Singhal, Shekoofeh Azizi, Tao Tu, S Sara Mahdavi, Jason Wei, Hyung Won Chung, Nathan Scales, Ajay Tanwani, Heather Cole-Lewis, Stephen Pfohl, et al. Large language models encode clinical knowledge. *Nature*, 620(7972):172–180, 2023. 2
- [29] Aakanksha Chowdhery, Sharan Narang, Jacob Devlin, Maarten Bosma, Gaurav Mishra, Adam Roberts, Paul Barham, Hyung Won Chung, Charles Sutton, Sebastian Gehrmann, et al. Palm: Scaling language modeling with pathways. *Journal of Machine Learning Research*, 24(240):1–113, 2023. 2
- [30] Yunxiang Li, Zihan Li, Kai Zhang, Ruilong Dan, Steve Jiang, and You Zhang. Chatdoctor: A medical chat model fine-tuned on a large language model meta-ai (llama) using medical domain knowledge. *Cureus*, 15(6), 2023. 3
- [31] Tianyu Han, Lisa C Adams, Jens-Michalis Papaioannou, Paul Grundmann, Tom Oberhauser, Alexander Löser, Daniel Truhn, and Keno K Bresslem. Medalpaca—an open-source collection of medical conversational ai models and training data. *arXiv preprint arXiv:2304.08247*, 2023. 3
- [32] Brandon McKinzie, Zhe Gan, Jean-Philippe Fauconnier, Sam Dodge, Bowen Zhang, Philipp Dufter, Dhruvi Shah, Xi-anzhi Du, Futang Peng, Anton Belyi, et al. Mm1: methods, analysis and insights from multimodal llm pre-training. In *European Conference on Computer Vision*, pages 304–323. Springer, 2024. 3
- [33] Shengbang Tong, Zhuang Liu, Yuexiang Zhai, Yi Ma, Yann LeCun, and Saining Xie. Eyes wide shut? exploring the visual shortcomings of multimodal llms. In *Proceedings of the IEEE/CVF Conference on Computer Vision and Pattern Recognition*, pages 9568–9578, 2024.
- [34] Hulingxiao He, Geng Li, Zijun Geng, Jinglin Xu, and Yuxin Peng. Analyzing and boosting the power of fine-grained visual recognition for multi-modal large language models. *arXiv preprint arXiv:2501.15140*, 2025. 3
- [35] Debjyoti Mondal, Suraj Modi, Subhadarshi Panda, Rituraj Singh, and Godawari Sudhakar Rao. Kam-cot: Knowledge augmented multimodal chain-of-thoughts reasoning. In *Proceedings of the AAAI conference on artificial intelligence*, volume 38, pages 18798–18806, 2024. 3
- [36] Hao Shao, Shengju Qian, Han Xiao, Guanglu Song, Zhuofan Zong, Letian Wang, Yu Liu, and Hongsheng Li. Visual cot: Advancing multi-modal language models with a comprehensive dataset and benchmark for chain-of-thought reasoning. *Advances in Neural Information Processing Systems*, 37:8612–8642, 2024.
- [37] Yanming Liu, Xinyue Peng, Tianyu Du, Jianwei Yin, Weihao Liu, and Xuhong Zhang. Era-cot: improving chain-of-thought through entity relationship analysis. *arXiv preprint arXiv:2403.06932*, 2024.
- [38] Jiachun Li, Pengfei Cao, Chenhao Wang, Zhuoran Jin, Yubo Chen, Daojian Zeng, Kang Liu, and Jun Zhao. Focus on your question! interpreting and mitigating toxic cot problems in commonsense reasoning. *arXiv preprint arXiv:2402.18344*, 2024. 3
- [39] Shih-Cheng Huang, Liyue Shen, Matthew P Lungren, and Serena Yeung. Gloria: A multimodal global-local representation learning framework for label-efficient medical image recognition. In *Proceedings of the IEEE/CVF International Conference on Computer Vision*, pages 3942–3951, 2021. 3, 7
- [40] Olivier Bodenreider. The unified medical language system (umls): integrating biomedical terminology. *Nucleic acids research*, 32(suppl_1):D267–D270, 2004. 3
- [41] Yuhao Zhang, Hang Jiang, Yasuhide Miura, Christopher D Manning, and Curtis P Langlotz. Contrastive learning of medical visual representations from paired images and text. In *Machine Learning for Healthcare Conference*, pages 2–25. PMLR, 2022. 7
- [42] Benedikt Boecking, Naoto Usuyama, Shruthi Bannur, Daniel C Castro, Anton Schwaighofer, Stephanie Hyland, Maria Wetscherek, Tristan Naumann, Aditya Nori, Javier Alvarez-Valle, et al. Making the most of text semantics to improve biomedical vision–language processing. In *European conference on computer vision*, pages 1–21. Springer, 2022. 7
- [43] Ekin Tiu, Ellie Talius, Pujan Patel, Curtis P Langlotz, Andrew Y Ng, and Pranav Rajpurkar. Expert-level detection of pathologies from unannotated chest x-ray images via

self-supervised learning. *Nature biomedical engineering*,
6(12):1399–1406, 2022. [7](#)